REPORT 1239

ERROR IN AIRSPEED MEASUREMENT DUE TO THE STATIC-PRESSURE FIELD AHEAD OF AN AIRPLANE AT TRANSONIC SPEEDS [1]

By Thomas C. O'Bryan, Edward C. B. Danforth, and J. Ford Johnston

SUMMARY

The magnitude and variation of the static-pressure error for various distances ahead of sharp-nose bodies and open-nose air inlets and for a distance of 1 chord ahead of the wing tip of a swept wing are defined by a combination of experiment and theory. The mechanism of the error is discussed in some detail to show the contributing factors that make up the error. The information presented provides a useful means for choosing a proper location for measurement of static pressure for most purposes.

INTRODUCTION

The precision with which airspeed and altitude can be measured in flight by a pitot-static tube depends upon the accuracy with which the free-stream total and static pressures are determined. The error introduced by a well-designed pitot-static airspeed head is usually negligible both at subsonic and at supersonic speeds (refs. 1 and 2). The problem is then resolved into the choice of a location for the airspeed head at which the total and static pressures are affected to a minimum extent by the pressure field of the airplane.

There is no difficulty in locating the total-pressure tube at subsonic speeds if it is placed well outside of the propeller slipstream, the boundary layer, and the wake from the airplane structure. At supersonic speeds, there is a loss in total pressure when the total-pressure tube is subjected to a shock wave; however, this loss is negligible at low supersonic speeds and may be calculated from the normal shock relations at higher speeds.

The location of static-pressure tubes for minimum static-pressure error can be realized at subsonic speeds by locating the tube sufficiently far ahead of the wing tip of the airplane (usually one chord length for research purposes). Satisfactory measurements may also be obtained in many instances by fuselage static vents. The choice of a suitable vent location, however, must usually be made by trial in wind-tunnel or flight tests.

Locations of static-pressure tubes that are satisfactory at subsonic speeds are usually unsuitable at transonic speeds, as they are subject to large and abrupt changes in indicated pressure. The problem at transonic speed is resolved into the choice of a location for the static-pressure tube that is far enough ahead of the airplane to give a static-pressure error that can be tolerated.

This report is a compilation of material from three separate NACA investigations [1] intended to show, from model tests, measurements of static-pressure error as well as a means of predicting the magnitude of the error at transonic speeds. The investigations were performed by means of the NACA wing-flow method (ref. 3) for a Mach number range of 0.70 to 1.10. Three locations of the static-pressure source, ahead of sharp-nose bodies (part I), ahead of an open-nose air inlet (part II), and ahead of the wing tip of a sweptback wing (part III) were investigated.

SYMBOLS

D	maximum diameter of body
d	inlet diameter
f, F, G	functions
K	a constant
l	twice nose length of body
M	Mach number
p	static pressure
p_∞	free-stream static pressure (at model position)
q	dynamic pressure
q_c	impact pressure
$\frac{\Delta p}{q_c}$	static-pressure error, $\frac{p-p_\infty}{q_c}$
V_i	velocity at inlet
V_∞	free-stream velocity
X	distance from inlet to maximum-diameter station
x	axial distance ahead of nose of body
γ	ratio of specific heat at constant pressure to specific heat at constant volume

I—MEASUREMENT OF STATIC PRESSURE AHEAD OF SHARP-NOSE BODIES OF REVOLUTION AT TRANSONIC SPEEDS

The development of jet and rocket engines for aircraft has permitted the design of relatively sharp-nose fuselages. Static-pressure tubes located a sufficient distance ahead of a sharp-nose fuselage have been found to furnish a measurement of static pressure subject to only a small error through-

[1] Supersedes NACA RM L9C25, 1949 by Edward C. B. Danforth and J. Ford Johnston, NACA RM L50L28, 1951 by Edward C. B. Danforth and Thomas C. O'Bryan, and NACA RM L52A17, 1952 by Thomas C. O'Bryan.

out the entire range of Mach number except for the pressure rise near the Mach number for passage of the bow wave.

The static-pressure error ahead of fuselage-like bodies at low subsonic speeds is reported in reference 4. It was shown that, at low Mach numbers, static-pressure errors of the order of 1.5 percent of stream impact pressure can be obtained at one diameter ahead of a sharp-nose body. At supersonic speeds, it is evident that the static-pressure error will be zero at all points ahead of the body bow wave. The static-pressure error will be zero, even at relatively short distances ahead of the fuselage, for all supersonic Mach numbers, except those very near 1.0. Thus, while the static-pressure error ahead of a fuselage nose was known to be small at subsonic and supersonic speeds, no information, either experimental or theoretical, was available for predicting the magnitude of the error at transonic speeds. For this reason, the investigation of reference 4 was extended to transonic speeds. This part of the investigation consisted of the measurement of the pressures at several distances ahead of two sharp-nose bodies of revolution at zero angle of attack between Mach numbers of 0.7 and 1.1.

MODELS

The general details of the two sharp-nose bodies of revolution used in this part of the investigation are shown in the photographs of figure 1 and the sketches of figure 2. The flush static-pressure orifices appearing in the photographs were used in another investigation and have no bearing on this part of the present report. Body A (fig. 1 (a)) was of circular-arc profile and fineness ratio 6. Body B had a larger nose angle than body A, and its maximum thickness was forward of midlength. The nose of body B (fig. 1 (b)) was equivalent to a body of fineness ratio 4.5 and was similar in shape to that of the X–1 airplane without the cockpit and nose landing-gear enclosures. Each body was equipped with a cone-pointed static-pressure tube of 0.060-inch diameter extending forward axially from the nose. This tube carried eight 0.010-inch-diameter orifices located 0.30 inch (five tube diameters) behind the shoulder of the cone point (called herein the "short-nose static-pressure tube"). Additional tests were carried out on body B with a similar tube having orifices located 1.20 inches (20 diameters) behind the shoulder (called the "long-nose static-pressure tube").

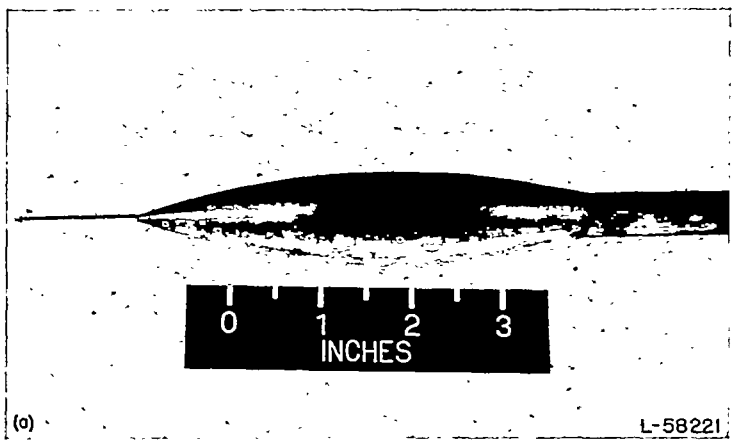

(a) Body A.

FIGURE 1.—Photographs of sharp-nose models.

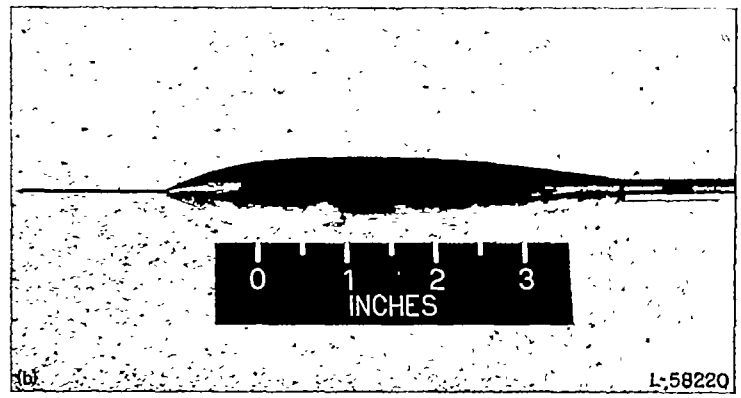

(b) Body B.

FIGURE 1.—Concluded.

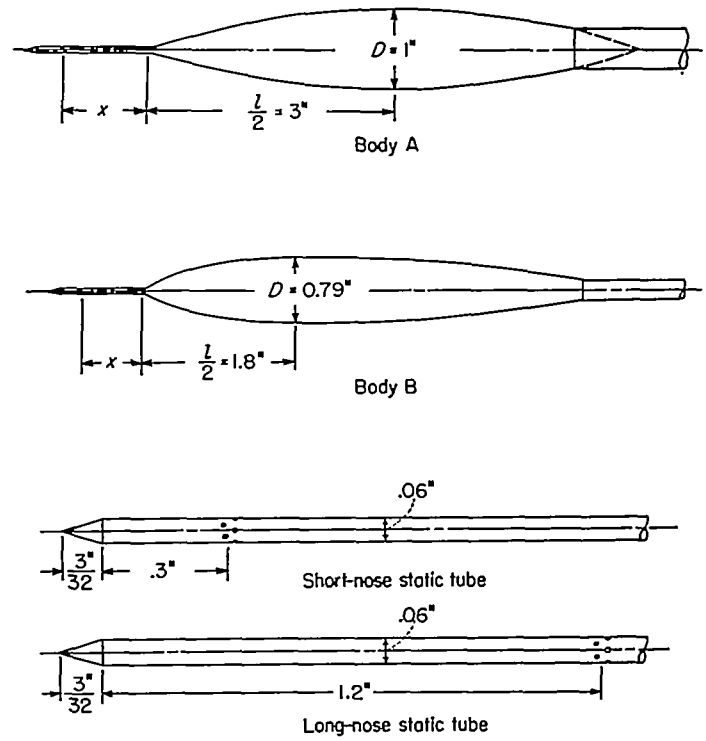

FIGURE 2.—Sketch of bodies and model static-pressure tubes.

METHOD

The static pressure at the model orifice position without the model in place was calibrated with respect to the static pressure at a reference location sufficiently forward and to the side of the model that it would be essentially unaffected by the model. The location of the static-pressure tube at the height of the model above the wing surface is shown in figures 3 and 4. The calibration is given in figure 5 in terms of static-pressure coefficient $\Delta p/q_o$ at the model location as a function of Mach number at the reference orifice. The static-pressure error due to body A or B was taken as the difference between the relative pressures at the reference location and at the test positions with and without the model in place.

The models were sting mounted, as shown in the photograph of body B in figure 6, at 6.25 inches above the airplane wing surface and were alined with the local flow.

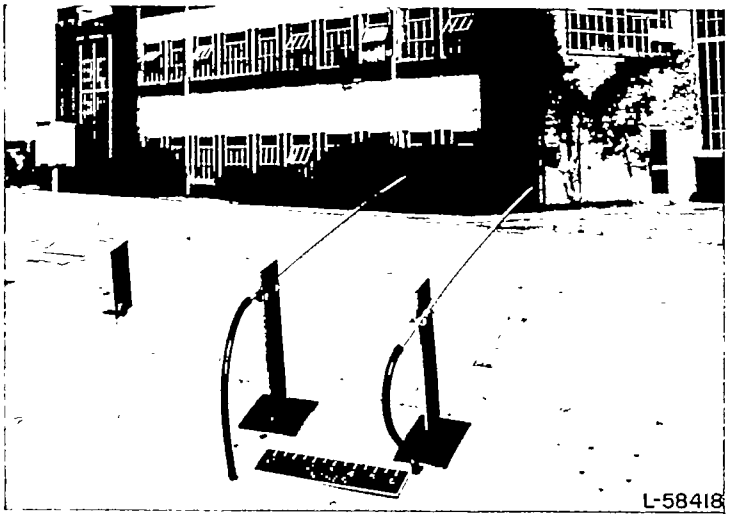

FIGURE 3.—Static-pressure tubes used in calibration.

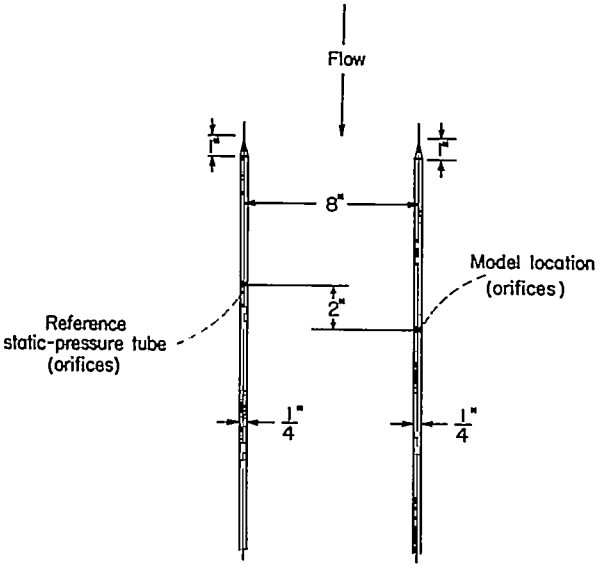

FIGURE 4.—Location of orifices used to calibrate test panel.

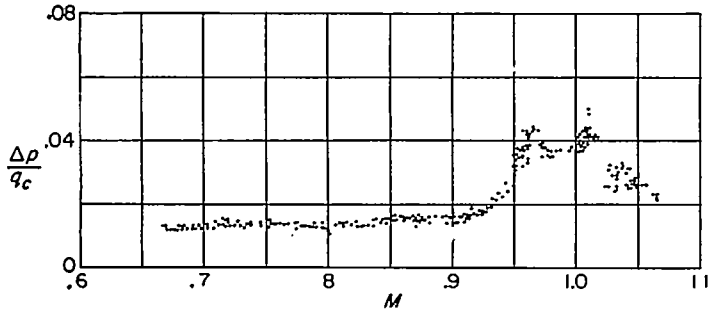

FIGURE 5.—Calibration of test panel.

The tests were conducted in dives from high altitude during which the Mach number at the model position varied from about 0.7 to 1.1. The differential pressures between the model orifice position and the two reference positions were measured by sensitive differential-pressure recorders. Other standard NACA instruments recorded the absolute pressure at the reference static-pressure tube and the airplane impact pressure.

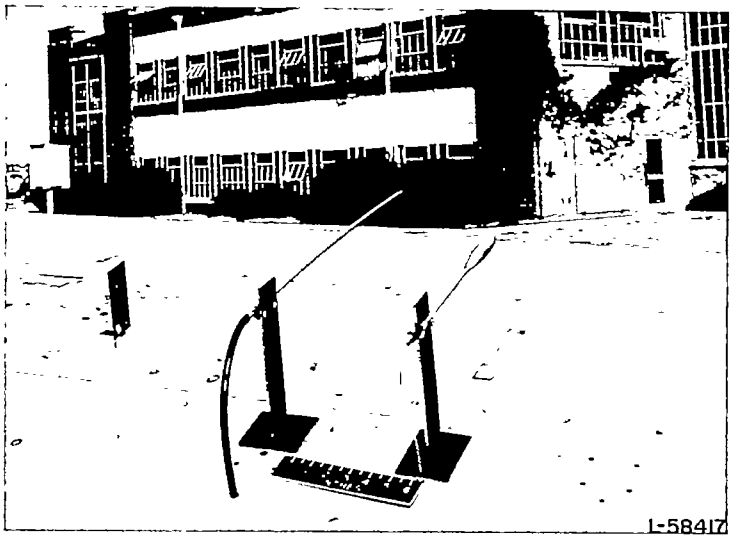

FIGURE 6.—Body B and reference static-pressure tube mounted on test panel.

Measurements of the static-pressure error have been made at distances of 0.6 and 1.5 body diameters ahead of body A and at 0.50, 0.75, and 1.7 body diameters ahead of body B. The bodies were moved relative to the pressure tube so that the orifice location would always be located at the same point. The static-pressure error of body A was obtained with the short-nose static-pressure tube only, while that of body B was obtained with both the short-nose and the long-nose tubes.

RESULTS AND DISCUSSION

VARIATION OF STATIC-PRESSURE ERROR WITH MACH NUMBER

The results of the measurements of static-pressure error for body A are shown in figure 7 at distances ahead of the nose x/D of 0.6 and 1.5 and for body B in figure 8 at distances x/D of 0.5, 0.75, and 1.7. The static-pressure error $\Delta p/q_c$ is presented as the error in static pressure expressed as a fraction of the true impact pressure q_c at the model orifice position and is shown as a function of the Mach number at that point.

Variation below body critical Mach number.—It can be seen in figures 7 and 8 that the static-pressure error is essentially constant at Mach numbers lower than about 0.9. This effect is predicted by the subsonic linearized theory (ref. 5), which shows that the static-pressure error on the axis of a body of revolution, either ahead of or behind the body, is independent of Mach number to the first order. The static-pressure errors ahead of the two bodies calculated by the subsonic linearized theory are represented in figures 7 and 8 by the triangular symbols. The experimental values of static-pressure error are expressed as a fraction of impact pressure q_c, whereas the theoretical values are expressed as a fraction of dynamic pressure q. The theoretical values of static-pressure error have been divided by the ratio q_c/q in order to provide the same basis of comparison. The agreement of the theoretical and measured errors is generally very satisfactory for Mach numbers up to 0.90. It would appear, therefore, that the bodies are sufficiently slender that they do not grossly violate the slender-body assumption of the linearized theory.

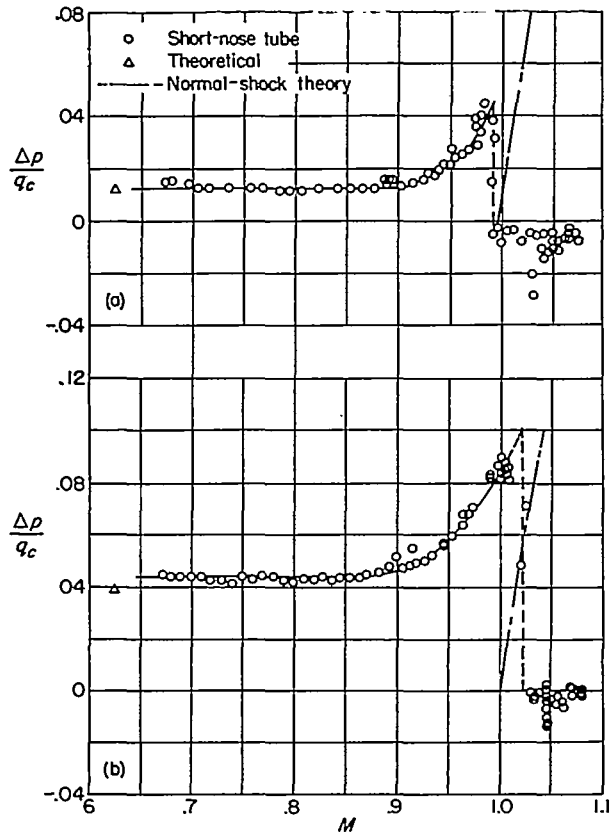

(a) $\frac{x}{D}$=1.5.

(b) $\frac{x}{D}$=0.6.

FIGURE 7.—Static-pressure error ahead of body A.

Variation above body critical Mach number.—Even for very slender bodies, the assumptions of the subsonic linearized theory become invalid if sonic speed is approached at some point on the body, and measurements are then expected to depart from the predictions of the theory. It was shown from pressure-distribution measurements of body A in reference 6 that sonic speed is first reached at the maximum-thickness position at a Mach number of about 0.92. The results of the present tests (fig. 7) show that, at approximately the same Mach number at which sonic speed is attained on the body, the static-pressure error of body A begins to deviate.

The increase in static-pressure error of bodies A and B at Mach numbers greater than about 0.9 (figs. 7 and 8) is associated with the development of a supersonic region near the maximum-thickness position of the body. The influence of the negative pressures on the body in this region cannot travel directly forward as at lower Mach numbers but must travel around the supersonic region or through the subsonic boundary layer and the pressure is thus considerably attenuated at the position of the model static-pressure orifices. The positive pressures near the nose of the body, however, are in a subsonic flow and are not attenuated. The net effect is an increase of the static-pressure error with Mach number to values that are large in comparison with the error at low Mach number. It should be noted, however, that, if the static-pressure orifices are located sufficiently far ahead of the nose of the body, the static-pressure error will be small at low Mach numbers and will remain reasonably small at all higher Mach numbers. For example, the static-pressure error at x/D=1.7 ahead of body B (fig. 8 (a)) varied from $0.015q_c$ to a peak of $0.040q_c$ as the Mach number increased from 0.9 to 1.0.

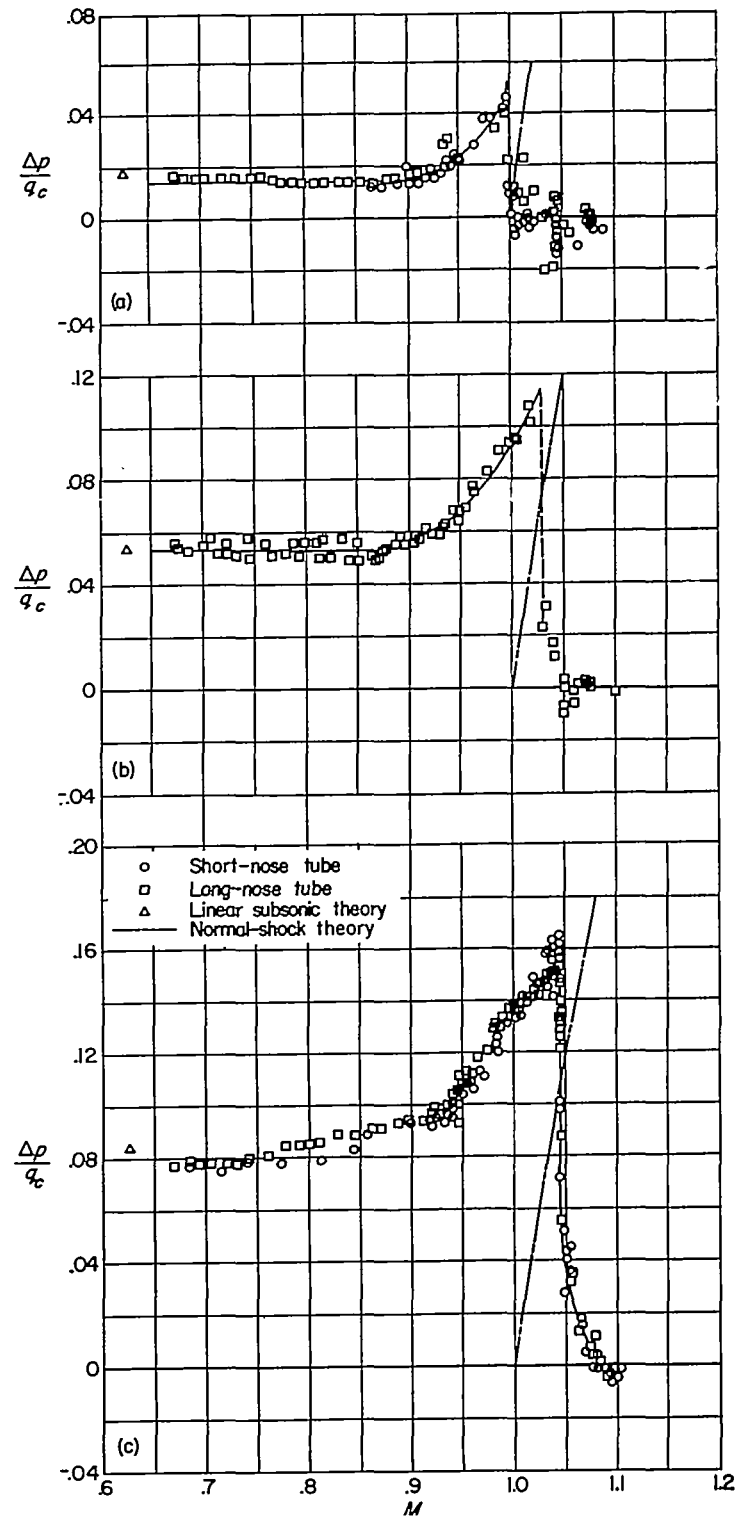

(a) $\frac{x}{D}$=1.7.

(b) $\frac{x}{D}$=0.75.

(c) $\frac{x}{D}$=0.5.

FIGURE 8.—Static-pressure error ahead of body B.

As the free-stream Mach number becomes supersonic, a shock wave forms far ahead of the body, and the pressure field of the body is terminated. With increasing supersonic speed, the pressure ahead of the body continues to increase, and the shock wave approaches the body. Finally, when the Mach number becomes sufficiently high, the shock wave passes over the orifices in the static-pressure tube. At this point, a sharp decrease in the pressure at the orifices (figs. 7 and 8) corresponding to the pressure change through a normal shock will occur, except as modified by the curvature and thickness of the shock and by boundary-layer shock interaction. At this and higher Mach numbers, the static-pressure orifices will be completely isolated from the field of the body and will indicate the static pressure of the free stream, as shown in figures 7 and 8. For example, the Mach number at which the shock passed the orifices of body B (fig. 8) varied from about 1.0 at $x/D=1.7$ to 1.05 at $x/D=0.5$.

Comparison of pressure discontinuity with normal-shock theory.—The theoretical variation with Mach number of the pressure coefficient $\Delta p/q_c$ across a normal shock is also shown in figures 7 and 8. For both bodies and at all positions of measurement, the discontinuity in pressure occurred at a Mach number approximately 0.02 lower than would be expected from the normal-shock theory. Conversely, at a given Mach number, the pressure rise through shock was about $0.04q_c$ greater than that indicated by theory. More startling is the appearance of a shock involving a pressure rise of $0.04q_c$ at a Mach number of 1.0 (figs. 7 (a) and 8 (a)), where the theory indicates that no finite shock should exist. This basic disagreement between theory and experiment made necessary a critical examination of the experimental technique as regards model interference, pressure lag, and instrumentation; however, no explanation for this disagreement was found.

VARIATION OF STATIC-PRESSURE ERROR WITH x/D

Variation below body critical Mach number.—The variation of $\Delta p/q_c$ with x/D for Mach numbers less than 0.9 (the body critical Mach number) is shown for bodies A and B in figure 9 (a). Data obtained at a low Mach number (ref. 4) for a circular-arc body of fineness ratio 8.3 have been included. The variations of $\Delta p/q_c$ with x/D calculated by the linearized subsonic theory for the three bodies have been plotted in figure 9 (a) for comparison. The theoretical values of the static-pressure error are in good agreement with the values measured at Mach numbers less than 0.9. It is seen that the static-pressure error varies with distance ahead of the nose, the error being small at distances far ahead of the body and large at short distances ahead of the body. In particular, the static-pressure error of body B was reduced from $0.08q_c$ at $x/D=0.5$ to only $0.015q_c$ at $x/D=1.7$.

Variation above body critical Mach number.—The maximum values of $\Delta p/q_c$ which occur above the body critical Mach number just prior to the passage of shock across the static orifices are shown for bodies A and B as a function of x/D in figure 9 (b). As in the case of variation of the error at Mach numbers below body critical, the peak error varies with distance ahead of the body and the magnitude decreases with increasing distance ahead of the body.

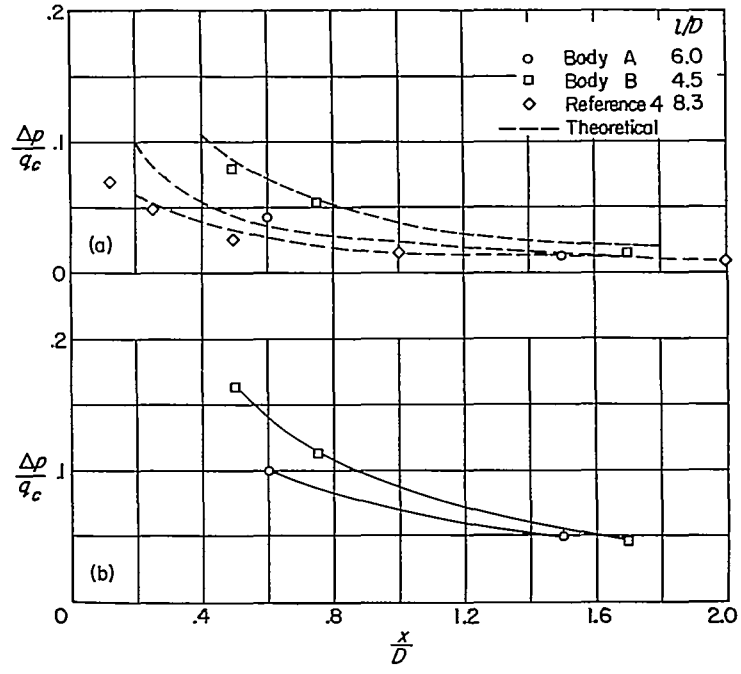

(a) Below body critical Mach number.

(b) Peak static-pressure error.

FIGURE 9.—Variation of position error with distance ahead of body nose.

CORRELATION FOR BODIES OF SIMILAR SHAPE

The data shown in figures 9 (a) and 9 (b) have been replotted in figures 10 (a) and 10 (c) as $\left(\frac{l}{D}\right)^2\frac{\Delta p}{q_c}$ as a function of x/l. In the case of body B, which was unsymmetrical fore and aft, the fineness ratio was calculated on the basis of twice the nose lengths, that is, the part of the body ahead of maximum thickness. This approximation is justified, since the forward part of the body is far more effective than the rear part in determining the magnitude of the static-pressure error ahead of the body.

Correlation below body critical Mach number.—The data at $M<0.9$ for bodies A and B and at lower speeds for the body tested in reference 4 all seem to correlate in figure 10 (a) along a single curve. It may be shown by the linearized subsonic theory (ref. 5) that, for bodies of revolution of the same family (that is, those having the same thickness distribution), the static-pressure error at a given fraction of the body length ahead of the nose is inversely proportional to the square of the fineness ratio $\left(\frac{l}{D}\right)^2$. Since bodies A and B and that of reference 4 are all closely parabolic, the variation of $\left(\frac{l}{D}\right)^2\frac{\Delta p}{q_c}$ with x/l calculated by the linearized subsonic theory for parabolic-arc bodies is shown in figure 10 (a) for comparison. The experimental data for Mach numbers below the body critical Mach number (less than 0.9) and for fineness ratios between 4.5 and 8.3 are seen to agree well with the theoretical curve.

Correlation above body critical Mach number.—The similarity law for axially symmetric transonic flow is discussed in reference 7, in which an expression is derived relating the pressure coefficients at similar points on the contours and axes of bodies of revolution with the same

thickness distribution. This expression with symbol-notation changes to agree with that used herein is:

$$\frac{\Delta p}{q}=\left(\frac{D}{l}\right)^2 f\left[\frac{\left(\frac{D}{l}\right)^2\frac{\gamma+1}{2}}{M-1},\frac{x}{l}\right] \tag{1}$$

For all cases in which the fluid is the same, the term $\frac{\gamma+1}{2}$ may be omitted. The first parameter becomes infinite at $M=1$ so that it will be more convenient to use its reciprocal. If, then, equation (1) is rearranged, we have

$$\left(\frac{l}{D}\right)^2\frac{\Delta p}{q}=F\left[\left(\frac{l}{D}\right)^2(M-1),\frac{x}{l}\right] \tag{2}$$

Equation (2) shows that all bodies with a given thickness distribution will, at equal values of x/l, exhibit the same variation of $\left(\frac{l}{D}\right)^2\frac{\Delta p}{q}$ with $\left(\frac{l}{D}\right)^2(M-1)$.

From cross plots of figures 7 and 8 at Mach numbers above 0.9, the data of bodies A and B have been replotted in figure 10 (b) with $\left(\frac{l}{D}\right)^2\frac{\Delta p}{q_c}$ as a function of $\left(\frac{l}{D}\right)^2(M-1)$ for several constant values of x/l and are seen to correlate in the manner predicted in equation (2). As discussed previously, the data in figure 10 (b) indicates that the bow waves pass the static orifices at Mach numbers less than those predicted by normal-shock theory.

Correlation of peak static-pressure error.—The peak values of the static-pressure error for bodies A and B shown in figure 9 (b) have been replotted in figure 10 (c) with $\left(\frac{l}{D}\right)^2\frac{\Delta p}{q_c}$ as a function of x/l and appear to correlate on a single curve in the same manner as was shown for the data obtained below the body critical Mach number. It will be shown that, for the particular case of peak static-pressure error, the transonic similarity law suggests exactly this correlation.

Equation (2) can be simplified for the case of the peak static-pressure error on the axis of the body. The peak value of $\Delta p/q$ is connected with M by the normal-shock relations, inasmuch as the peak value occurs just behind a normal shock. For slightly supersonic Mach numbers, $\Delta p/q$ across a normal shock varies approximately linearly with $M-1$ (linear for observed as well as theoretical), so that $M-1$ may be replaced by $K\frac{\Delta p}{q}$, where K is a constant. Equation (2) then becomes

$$\left(\frac{l}{D}\right)^2\frac{\Delta p}{q}=F\left[K\left(\frac{l}{D}\right)^2\frac{\Delta p}{q},\frac{x}{l}\right]$$

or

$$G\left[\left(\frac{l}{D}\right)^2\frac{\Delta p}{q},\frac{x}{l}\right]=0 \tag{3}$$

Equation (3) defines a single curve in the ordinates of figure 10 (c) and therefore corroborates the observed correlation of the peak static-pressure errors for bodies A and B.

Application of correlation.—For bodies with fineness ratio different from those tested, an estimate of the low-speed and peak static-pressure errors can be made from figures 10 (a) and 10 (c) provided the profile of the body nose is a reasonable approximation to a parabolic arc. In order to find the length of airspeed boom for use on a parabolic body to give a peak static-pressure error of a given magnitude, the peak-static-pressure-error curve in figure 10 (c) indicates the length in maximum body diameters. From figure 10 (a) the corresponding low-speed static-pressure error is found. The transition of the static-pressure error from the low-speed value to the peak value can be determined as a function of Mach number from figure 10 (b). With this final step, the complete static-pressure-error curve for all Mach numbers is determined, inasmuch as the static-pressure error at Mach numbers above that for shock passage is zero. These results should be valid for fineness ratios l/D at least as low as 4.5 and for distances ahead of the nose x/l as small as 0.1. The upper limits of these values of l/D and x/l are presumed to be unrestricted.

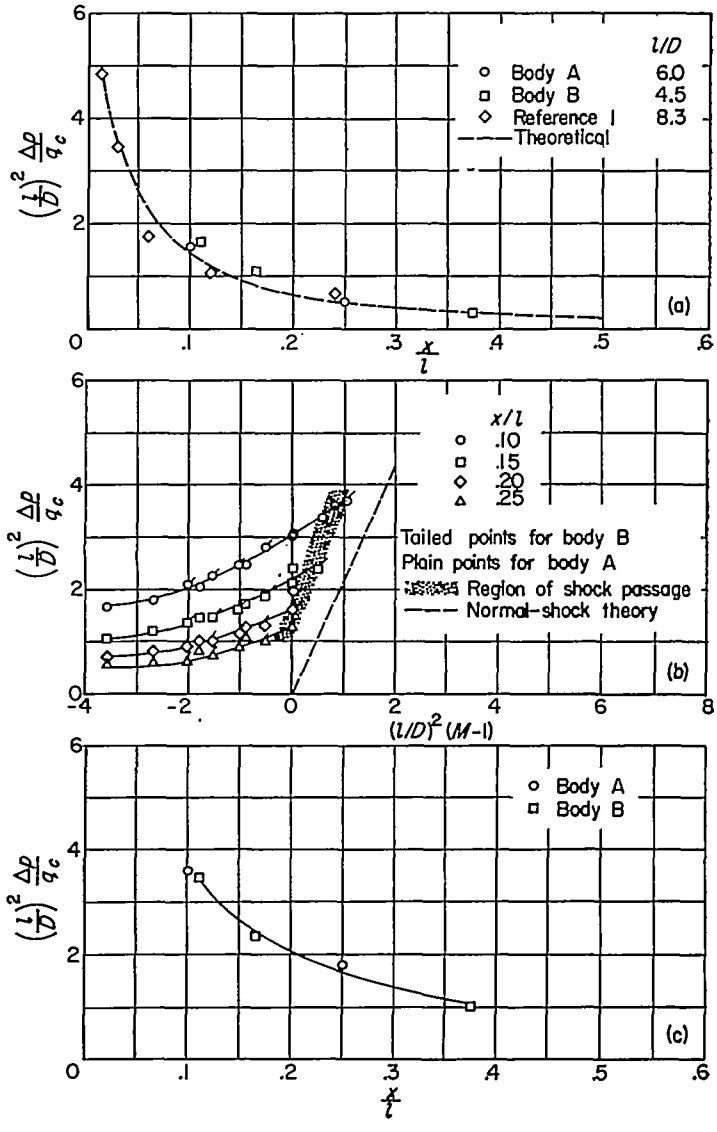

(a) Below body critical Mach number.
(b) Above body critical Mach number.
(c) Peak static-pressure error (just prior to shock passage).

FIGURE 10.—Correlation for bodies of a given thickness distribution.

II—MEASUREMENT OF STATIC PRESSURE AHEAD OF OPEN-NOSE AIR-INLET MODEL AT TRANSONIC SPEEDS

A variation of the fuselage nose installation was investigated, in which the static pressure was measured ahead of an open-nose air inlet. This configuration differs from the sharp-nose body used in part I, not only in bluntness at the nose, but also in the provision for variable air flow through the inlet. Results of the investigation are presented as variations with Mach number of the static-pressure error at several positions ahead of an open-nose air inlet for a small range of inlet-velocity ratios. The experimental results for $M=0.70$ are compared with theoretical calculations for incompressible flow and results of further computations are presented to provide information on the effect of changing inlet geometry.

MODEL

The model used for part II of this investigation, shown in a photograph in figure 11 and in a drawing giving details and dimensions in figure 12, was a nose-air-inlet body mounted centrally on a sting. The forebody was an NACA 1–50–150 inlet fairing into an elliptical afterbody. The body was equipped with a static-pressure probe identical to the short-nose pressure tube described in part I. One 0.020-inch orifice was located on the sting, which was in the inlet 0.88 inch behind the nose. This orifice measured the static pressure in the duct, from which inlet-velocity ratios V_i/V_∞ were obtained. Modifications to the model were made to change the inlet-velocity ratio for different tests. The inlet-velocity ratio was decreased by restricting the exit area with a plug.

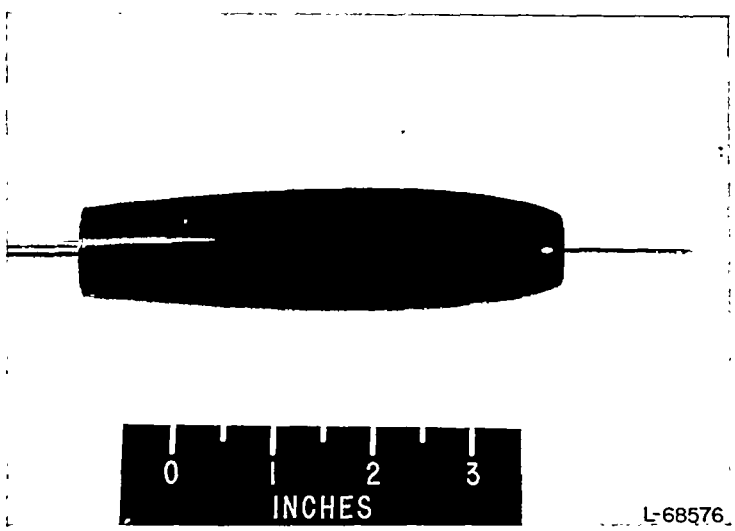

FIGURE 11.—Photograph of inlet model.

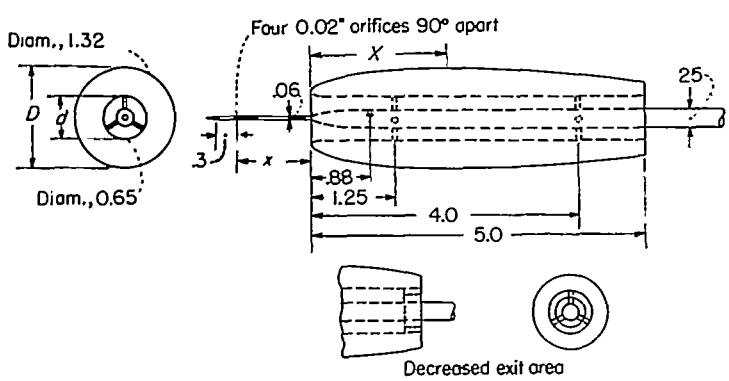

FIGURE 12.—Sketch of inlet model and modifications. (All dimensions are in inches.)

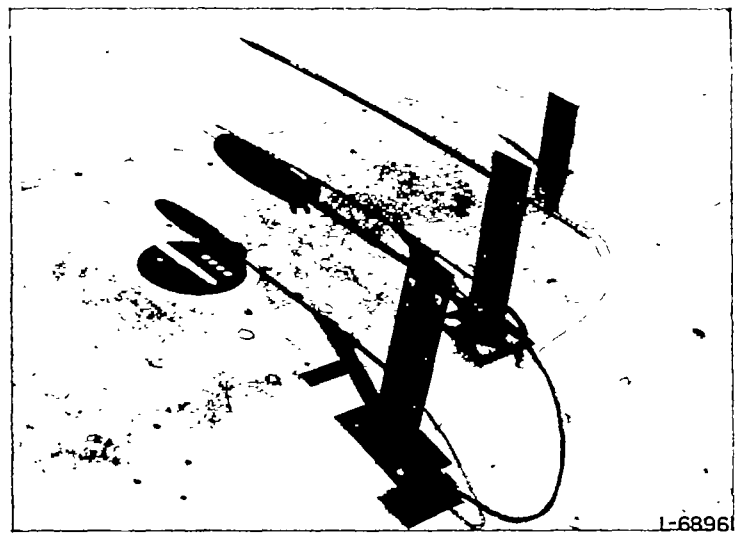

FIGURE 13.—Photograph of inlet model and reference static-pressure tube mounted on test panel.

METHOD

A photograph of the model mounted over the ammunition compartment door on the F–51 airplane is shown as figure 13. The model was mounted 6 inches above and parallel to the test panel and was alined with the local flow.

The static pressure measured at the positions of the orifices on the nose boom and the orifice in the duct, without the model in place, was calibrated with respect to the static pressure measured by a reference tube in the same manner as discussed in part I. The inlet-velocity ratio was calculated by the method of reference 8 on the basis of the measured static pressure in the duct and the free-stream Mach number.

RESULTS AND DISCUSSION

EXPERIMENTAL

The variations of inlet-velocity ratio with Mach number for the tests made with the static-pressure orifices at 1.5 and 4.0 inlet diameters ahead of the inlet (the only positions for which inlet-velocity ratio was determined) are shown in figure 14. The differences in inlet-velocity ratio for different locations of the static-pressure measurement ahead of the inlet with the original exit area are small and it is presumed that the same small variations would be measured for the intermediate locations of static-pressure measurement ahead of the inlet.

The variation of static-pressure error with Mach number at several positions ahead of the inlet is shown in figure 15. The inlet-velocity ratios for this configuration vary from about 0.68 at $M=0.70$ to 0.50 at $M=1.10$. The static-pressure error is relatively independent of Mach number below 0.90 and varies inversely with distance ahead of the inlet. For Mach numbers above 0.90 the static-pressure error rises rapidly; the peak error varies with distance

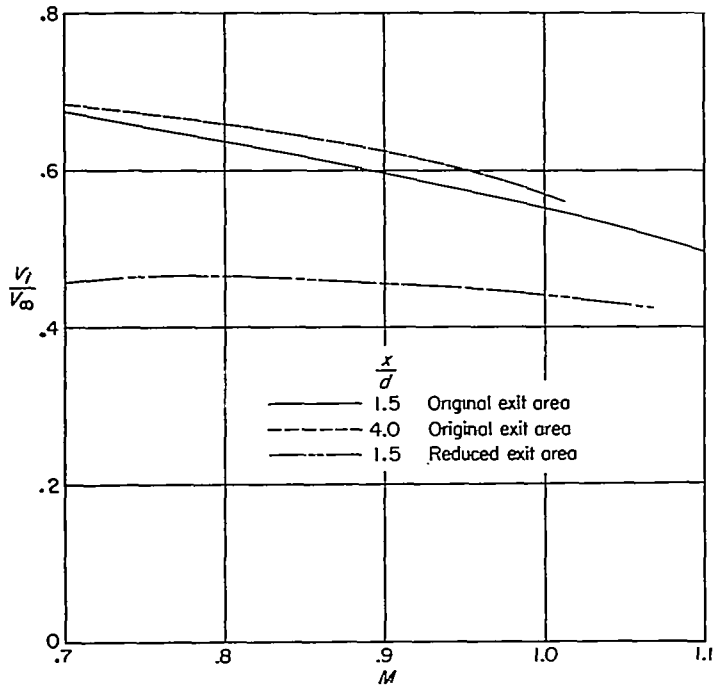

FIGURE 14.—Variation of inlet-velocity ratio with Mach number.

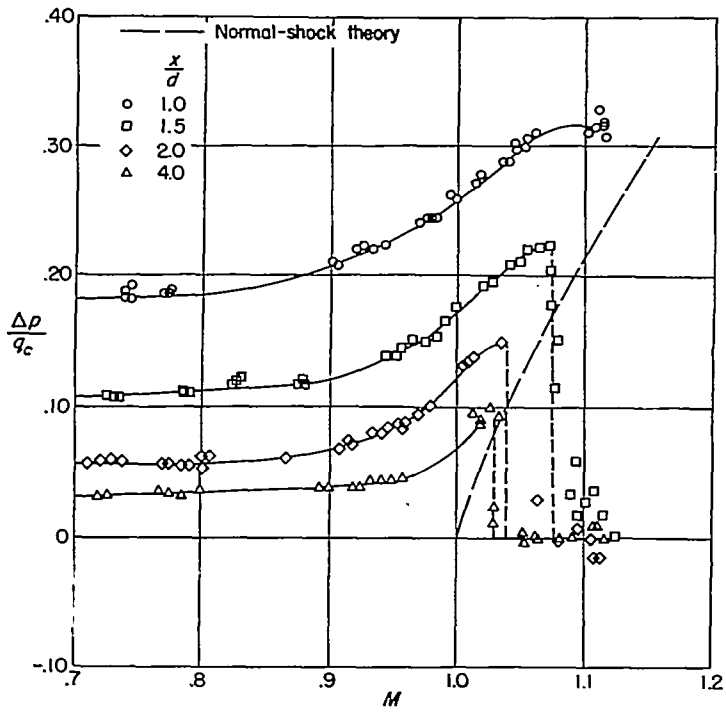

FIGURE 15.—Variation of static-pressure error ahead of inlet.

ahead of the nose, and the error is small at distances far ahead of the body and large at short distances ahead of the body. The static-pressure error continues to rise until the Mach number at which the body bow wave crosses the orifices is reached, whereupon the static-pressure error drops abruptly to zero.

The variation with Mach number of the static-pressure error across a normal shock, shown in figure 15, indicates that the pressure discontinuity occurred at a lower Mach number (approximately 0.02) than that predicted by normal-shock theory. This disagreement between theory and experiment is similar to that discussed previously in part I.

The effect of inlet-velocity ratio on the static-pressure error 1.5 inlet diameters ahead of the inlet is shown in figure 16 as a function of Mach number. The configuration for reduced inlet-velocity ratio is seen in figure 14 to have resulted in an average decrease of 0.1 inlet-velocity ratio for the Mach number range covered. The effect of this decrease in inlet velocity on the static pressure ahead of the inlet (fig. 16) resulted in an increase of approximately 0.02 in the static-pressure error throughout the Mach number range. The Mach number for shock passage was increased approximately 0.02.

EFFECT OF INLET GEOMETRY

In order to determine the effect of inlet geometry on the static-pressure error ahead of open-nose inlets, theoretical calculations were made of the static-pressure error (in this case, $\Delta p/q$) at several locations ahead of a number of NACA 1-series open-nose air inlets. A method is presented in reference 9 whereby the static-pressure error ahead of open-nose inlets in incompressible flow may be calculated by using experimental surface pressure distributions. The theoretical calculations were made at zero angle of attack for the inlets; the surface pressure distributions of reference 10 were utilized for this purpose.

Figure 17 presents the calculated variation of static-pressure error ahead of three NACA 1-series inlets of constant ratio of inlet diameter to maximum diameter ($d/D=0.5$) at several locations ahead of the inlet, for a range of inlet-velocity ratio V_i/V_∞ from 0.2 to 1.0. The designation of the inlet is descriptive of its geometric characteristics. (See ref. 10.) The first number ahead of the dash indicates the particular inlet series; the number between the two dashes indicates the ratio (in percent) of the inlet diameter d to the maximum body diameter D; the last number in the designation represents the ratio of (in percent) the inlet length X to the maximum diameter D. For example, the 1–50–100 inlet has a diameter ratio d/D of 0.5 and a length-diameter ratio X/D of 1.00. It is clear from figure 17 that, for the 1-series inlets having constant ratio of inlet diameter to

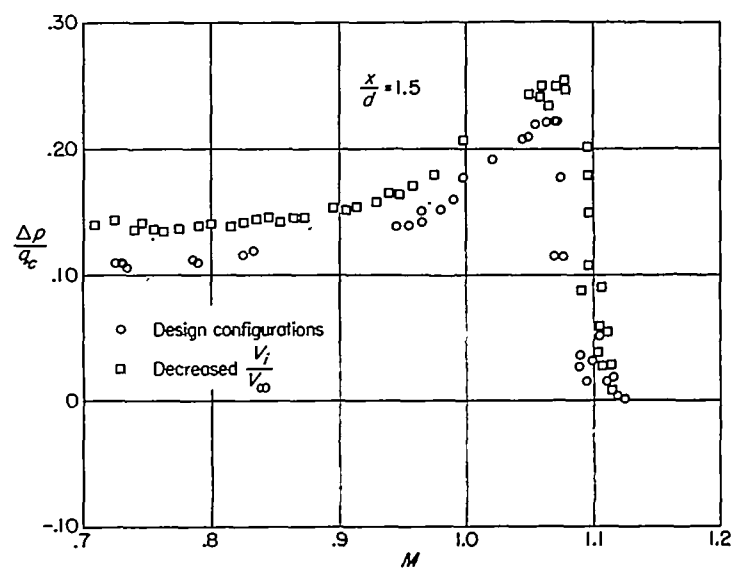

FIGURE 16.—Effect of inlet-velocity ratio on static-pressure error ahead of inlet.

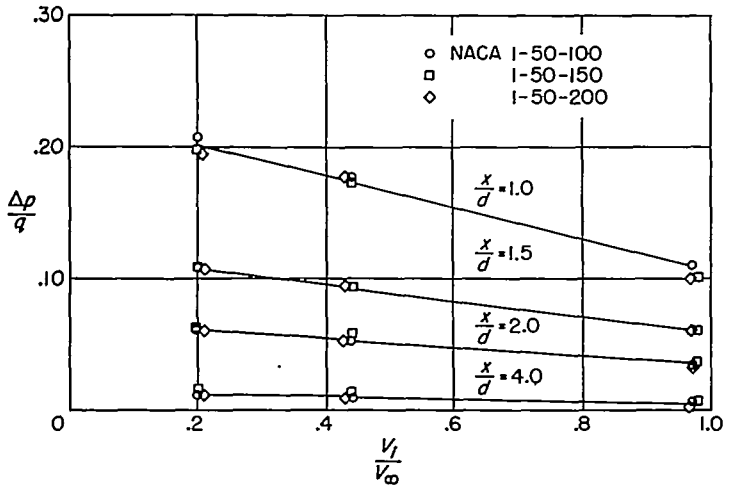

FIGURE 17.—Calculated variation of static-pressure error with inlet-velocity ratio at a number of inlet diameters ahead of three NACA series 1 inlets (1–50–100, 1–50–150, 1–50–200).

maximum diameter, the pressure ahead of the inlets is a function only of inlet-velocity ratio and location x/d ahead of the inlet. The static-pressure error ahead of the inlet is apparently independent of the length factor X/D. The most pronounced variation in pressure coefficient with inlet-velocity ratio occurred close to the inlet, as is evidenced by the slope of the pressure-error curve obtained from the location 1 inlet diameter ahead of the inlet. The magnitude of the variation of static-pressure error with inlet-velocity ratio decreased with distance ahead of the inlet until $\left(\text{at } \frac{x}{d}=4.0\right)$ the static-pressure error varied only from 0.005 to 0.01 as the inlet-velocity ratio was decreased from 1.0 to 0.2. At all values of x/d shown on figure 17, a reduction of inlet-velocity ratio from 1.0 to 0.2 caused the static-pressure error ahead of the inlet approximately to double.

The static-pressure error ahead of three 1-series inlets, in which the ratios of inlet diameter to maximum diameter and of maximum diameter to length were varied, is presented in figure 18. It is apparent from figure 18 that, as the inlet increases in diameter with respect to the maximum diameter, the static-pressure error decreases for a given inlet-velocity ratio and that this decrease is most pronounced for the position nearest the inlet. This analysis neglects the consideration of the effect of differences in the ratio of length to maximum diameter; however, it was shown in figure 17 that changes in this ratio had no effect on the pressure ahead of the inlet

COMPARISON WITH THEORY

The effect of an NACA 1–50–150 nose inlet on the static-pressure error at several locations ahead of the inlet is compared with calculations made by the theory of reference 9 in figure 19. The experimental data are those obtained by using the original configuration with measurements taken at 1.0, 1.5, 2.0, and 4.0 inlet diameters ahead of the inlet. The experimental data used were for the lowest Mach number of the test (M=0.70) and for an inlet-velocity ratio of 0.68.

The comparison in figure 19 indicates that the theory underestimates the measured static-pressure error an average of $0.025q_c$.

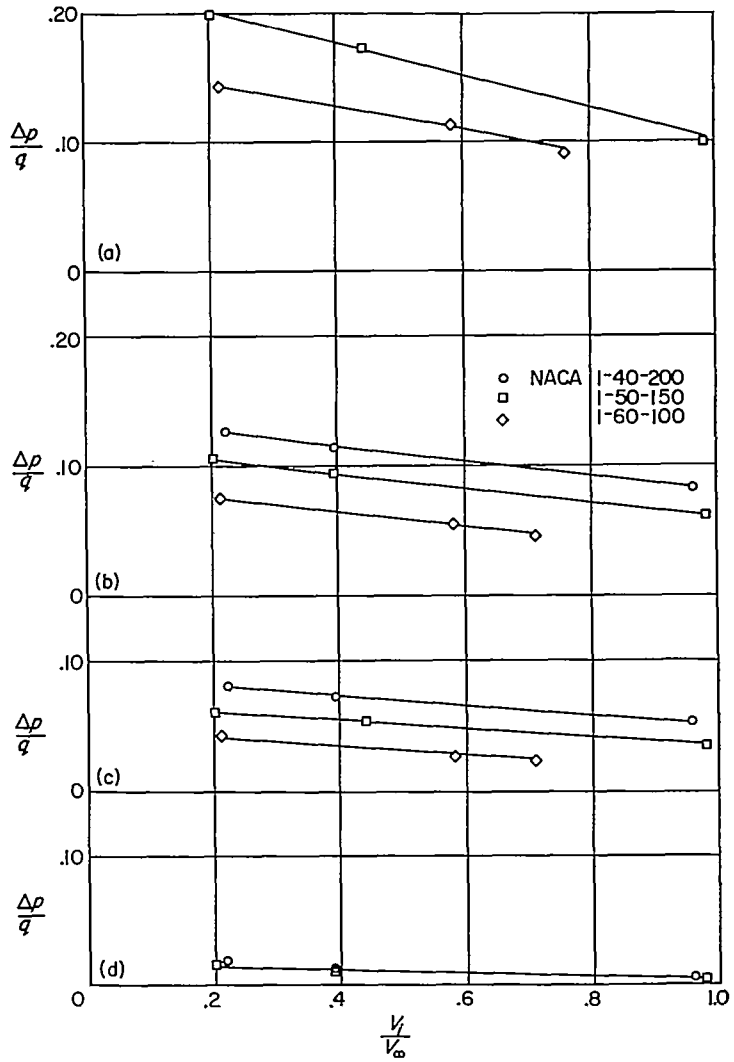

(a) $\frac{x}{d}$=1.0.

(b) $\frac{x}{d}$=1.5.

(c) $\frac{x}{d}$=2.0.

(d) $\frac{x}{d}$=4.0.

FIGURE 18.—Calculated variation of static-pressure error with inlet-velocity ratio at a number of inlet diameters ahead of three NACA series 1 inlets (1–40–200, 1–50–150, 1–60–100).

ESTIMATION OF PRESSURE ERROR

The static-pressure error to be expected ahead of inlets in incompressible flow can be estimated from figures 17 and 18. It has been shown in figure 19 that the theoretical variation of static-pressure error with distance ahead of the inlet, for incompressible flow, agreed within $0.025q_c$ with the experimental variation obtained from the NACA 1–50–150 inlet at a Mach number of 0.7. In order to validate the comparison the incompressible-theory values have been divided by the ratio q_c/q. The results of the incompressible-flow theory (ref. 9) given in figures 17 and 18 are therefore presumed to give the approximate static-pressure error to be expected ahead of other 1-series inlets at a Mach number of 0.7. If a knowledge of the low-speed pressure error is thus obtained, figure 15 can be used to estimate the increase

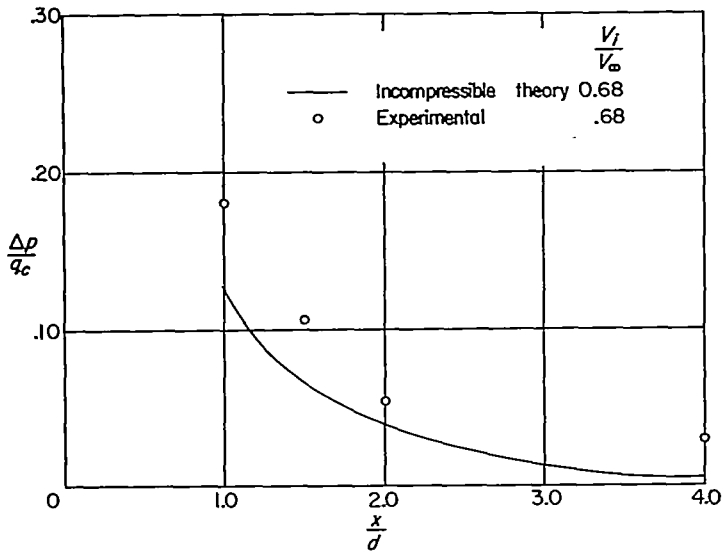

FIGURE 19.—Comparison of the experimental result of Mach number 0.70 with static-pressure error ahead of the inlet as calculated from reference 9.

in pressure to be expected at transonic speeds and the Mach number at which to expect the fuselage bow wave to cross the static-pressure orifices.

III—MEASUREMENT OF STATIC PRESSURE AHEAD OF THE WING TIP OF A SWEPT-WING AIRPLANE MODEL AT TRANSONIC SPEEDS

Airspeed installations ahead of fuselages have been shown to have acceptable calibrations at transonic speed. There are instances where the requirements of armament, radar, or propeller prohibit the location of a static-pressure tube ahead of the fuselage. For these cases static-pressure tubes are sometimes located ahead of the wing tip of an airplane.

Measurements of the static pressure at 1 chord ahead of the wing-tip leading edge of a half model of a swept-wing fighter airplane at or near zero lift are presented to show the magnitude of the static-pressure error to be expected for this position at transonic speeds. The mechanism and the variation of the error with Mach number are interpreted where possible by the linearized theory.

APPARATUS

A sketch showing a semispan model of a swept-wing fighter airplane mounted on the end plate used in the tests is presented as figure 20. A photograph of the model mounted on the wing-flow test panel and alined with the local flow direction is shown as figure 21.

The wing of the model was of aspect ratio 4.5 and taper ratio 0.28 with the quarter-chord line swept back 35°. The airfoil section outboard of the wing-root inlet was an NACA 65–009 section in planes normal to the quarter-chord line. The fuselage of the model was of fineness ratio 8.3 with the maximum diameter (excluding cockpit enclosure) located near its midlength position.

A static-pressure tube was attached to the wing tip of the model to simulate an airspeed boom, as shown in figures 20 and 21. The orifices in the static-pressure probe were

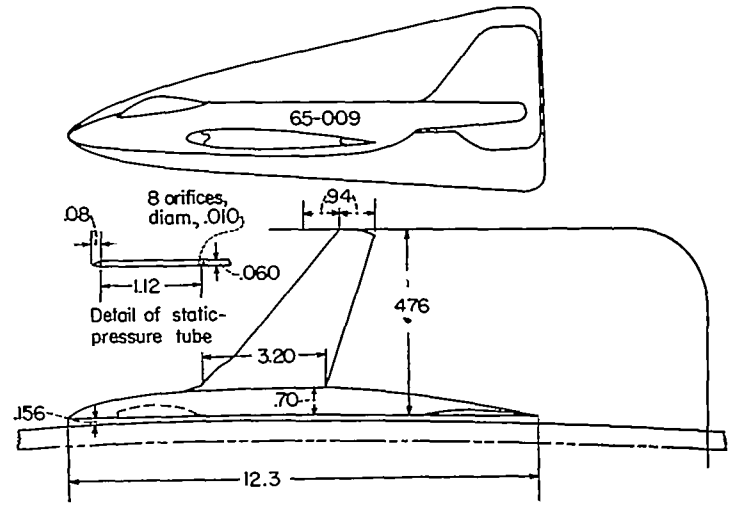

FIGURE 20.—Semispan model of swept-wing fighter airplane showing location of static orifices on wing-tip boom. (All dimensions are in inches.)

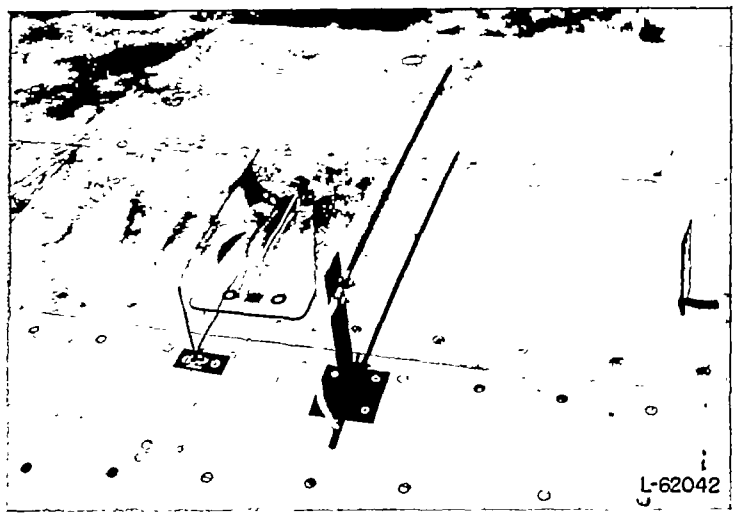

FIGURE 21.—Semispan model of swept-wing fighter airplane mounted on test panel.

located at 1 tip chord ahead of the wing-tip leading edge and 3.4 fuselage diameters outboard of the fuselage center line directly opposite the position of maximum fuselage diameter.

METHOD

Three model configurations were tested as follows: the end plate alone, the fuselage mounted on the end plate, and the complete model (wing and fuselage) mounted on the end plate.

The Mach number and static pressure at the model position are defined as those values measured at the orifices in the model airspeed boom from the tests of the end plate alone. For the other two configurations, the Mach number and the change in static pressure due to the presence of the fuselage were obtained by comparison with the data for the end plate alone at equal values of flight Mach number.

The static-pressure tube shown to the right of the model in figure 2 was intended to provide a reference Mach number as in parts I and II of this report. However, in the present part of the investigation, interference from the relatively large fuselage plus wing model made the indication of the reference pressure tube unreliable and necessitated the use

of the flight Mach number as a reference. This method is considered less accurate than the previous method but is believed to be sufficiently accurate to establish the magnitude of the error in static pressure caused by the model and the manner in which these errors vary with Mach number.

It should be kept in mind throughout the discussion that the method of mounting the model with the wing span perpendicular to the airplane-wing surface results in a decrease in stream Mach number at the model of about 0.04 from the root of the wing to the tip. The results of the measurements should, therefore, be expected to differ somewhat from results obtained with a uniform stream, as in flight. The nonuniformity of the stream would be expected to make less abrupt the variation of pressure ahead of the wing with Mach number. In all cases the Mach numbers quoted are the Mach numbers at the wing-tip position.

RESULTS AND DISCUSSION

The results of the investigation are shown in figure 22 as the variation of static-pressure error with Mach number. The pressure error ahead of the wing tip may be thought of as the algebraic sum of the pressure errors existing in the flow fields of the wing and fuselage taken separately. The tail surfaces are considered to have a negligible effect on the static pressure ahead of the wing tip. In order to separate the static-pressure error ahead of the wing tip into its major components, the static pressure at this point has been measured with the wing removed to determine directly the pressure error due to the fuselage. The separate pressure error due to the wing was not measured directly but was obtained by subtraction and thus includes any effect of wing-fuselage interference.

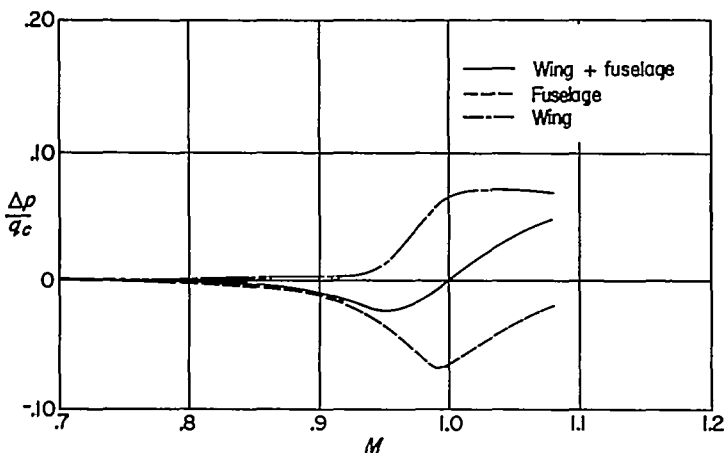

FIGURE 22.—Static-pressure error at wing-tip boom for wing plus fuselage, fuselage alone, and wing alone.

EFFECT OF FUSELAGE

The geometry of the model configuration was such that the static pressure was measured at 3.4 fuselage diameters outboard of the fuselage center line at a point directly opposite the position of maximum fuselage diameter. The fuselage would be expected to produce a negative pressure coefficient at this point of its flow field at all subsonic Mach numbers. The results in figure 22 show that, within the accuracy of measurement, the effect of the fuselage was negligible at Mach numbers below about 0.8. As the Mach number was increased above 0.8, however, the pressure coefficient due to the fuselage became rapidly negative, because of the pronounced lateral expansion of the pressure field of the fuselage that is known to take place at high subsonic speeds, and reached a maximum negative value of 0.07 near a Mach number of 1.0. As the Mach number increased above 1.0, the static-pressure error became less negative and reached a value of −0.02 at a Mach number of 1.08. This positive increase in static-pressure error at supersonic speeds may be explained by the simplified description of the flow field provided by the supersonic linearized theory. The pressures at points on the surface of the body are considered to be felt laterally only within the downstream Mach cones from those points on the body. These Mach cones become more and more sweptback as the Mach number is increased. The pressure at the point opposite the maximum-thickness position of the fuselage, therefore, becomes influenced more by the positive pressures near the fuselage nose and less by the negative pressures farther to the rear with the result that the pressure coefficient increases positively with Mach number.

The static-pressure error calculated by the linearized theory (ref. 11) at a point in the flow about a sharp-nose body of revolution with parabolic thickness distribution is shown as a function of Mach number in figure 23. The point chosen was in the same relative position with respect to the parabolic body as the point of static-pressure measurement with respect to the model fuselage. The fineness ratio of the parabolic body was equivalent to that of the model fuselage. The type of variation of the static-pressure error with Mach number is generally similar (fig. 23) for experiment and theory within the range of the test data except, of course, very near a Mach number of 1.0 where the linear theory predicts an infinite pressure coefficient.

The theoretical results for the simple parabolic body can be used to show qualitatively the variation of the pressure coefficient to be expected beyond the limit of the test data. The computed pressure coefficient of the parabolic body is seen (fig. 23) to increase to a maximum of 0.05 at a Mach number of 1.4 and to decrease smoothly thereafter, reaching zero at a Mach number of 1.62 as the Mach line from the body nose passes behind the point at which the pressure was calculated. The smooth decrease of the pressure error to

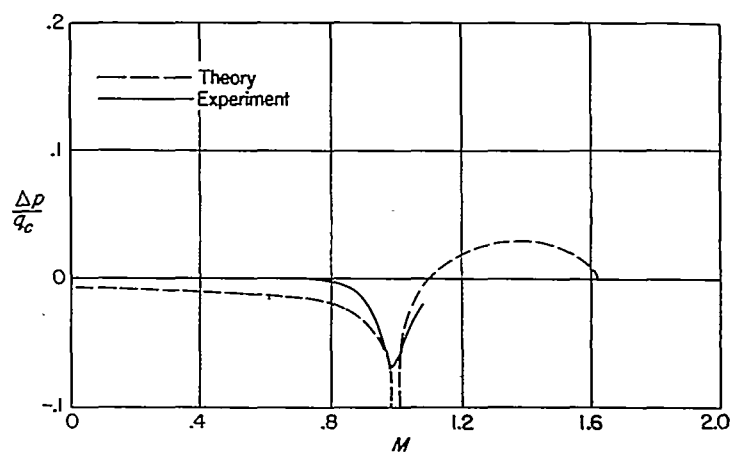

FIGURE 23.—Comparison of experimentally obtained variation with Mach number of the static-pressure error due to the fuselage with results obtained by the linearized theory.

zero would not occur experimentally, inasmuch as a bow wave, of which the linearized theory can take no account, will lie ahead of the Mach line from the body nose. The static-pressure error due to the model fuselage would therefore, in practice, drop abruptly to zero as the bow wave passes the static-pressure orifices. The Mach number for the passage of the bow wave would be somewhat higher than the value of 1.62 corresponding to the passage of the bow wave.

EFFECT OF WING

The static-pressure error produced by the wing at a point 1 chord ahead of the wing-tip leading edge is shown as a function of Mach number in figure 22. It is seen in figure 22 that the static-pressure error due to the wing was negligible at Mach numbers below about 0.92. Between the Mach numbers of 0.92 and 1.0, however, the static-pressure error increased rapidly to 0.07, and remained constant at this value, within the accuracy of measurement, to a Mach number of 1.08.

The static-pressure error has been calculated by the linearized nonlifting wing theory (refs. 12 and 13) at 1 tip chord ahead of the tip of a wing with the plan form and thickness ratio of the model wing but with double-wedge airfoil sections. The theoretical and experimental static-pressure errors are compared as functions of Mach number in figure 24. The theory is seen to predict a very small positive static-pressure error at low subsonic speeds which increases slightly with Mach number to 0.011 at a Mach number of 1. The measured pressure error is small and of the order of that predicted by theory at Mach numbers below about 0.92. At Mach numbers above 0.92, however, the differences between theory and experiment become marked. Such disagreement between linear theory and experiment is to be expected at transonic Mach numbers since the occurrence of mixed flow invalidates the assumptions of the theory.

The theoretical pressure is highly positive (infinite) at $M=1.0$ and decreases to high negative values at slightly supersonic speeds as the result of the loss, at the point ahead of the wing tip, of the effect of the positive pressures near the wing trailing edge. With further increase in Mach number the pressure ahead of the wing increases to positive values as the effect of the negative pressures behind the maximum-thickness line is lost. With still further increase in Mach number the positive pressures ahead of maximum thickness progressively lose their effect ahead of the wing tip and the pressure at that point decreases to zero and remains zero for all higher Mach numbers.

The mechanism of the rapid rise in static-pressure error due to the wing, which was found experimentally to take place subsonically at Mach numbers between 0.92 and 1.00, must be qualitatively similar to the overall change in the theoretical static-pressure error occurring supersonically between $M=1.00$ and $M=1.08$ although the sequence of the changes differs for experiment and theory. In the actual flow, as the critical Mach number of the airfoil sections is exceeded, a region of supersonic flow followed by shock forms near the maximum-thickness position with the result that, at points ahead of the wing, the effect of the negative pressures behind maximum thickness and the effect of the

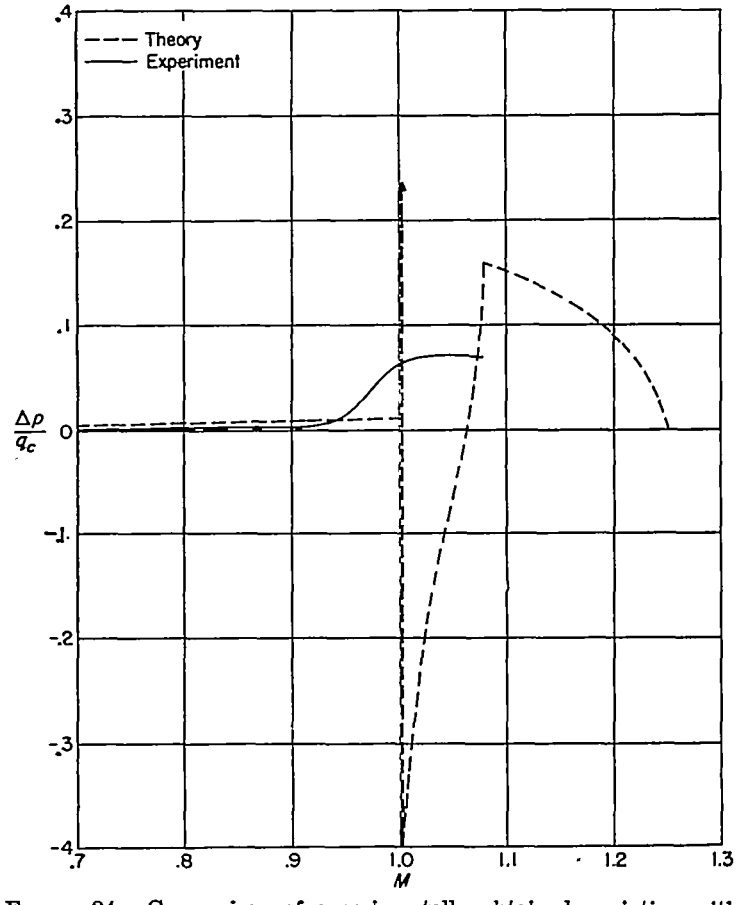

FIGURE 24.—Comparison of experimentally obtained variation with Mach number of the static-pressure error due to the wing with results obtained by the linearized theory.

positive pressures near the trailing edge are lost simultaneously. The loss in the effect of the negative pressures predominates so that the pressure error ahead of the wing increases positively.

According to the simple theory of swept wings of infinite span, the pressure coefficient ahead of the wing depends not upon the stream Mach number but upon the component of stream Mach number normal to the line of sweep. The predicted section critical Mach number of the NACA 65–009 airfoil is shown in reference 14 to be about 0.75 at a lift coefficient of 0.1. The corresponding critical stream Mach number for a 35° yawed infinite-span wing is, then, about 0.92 which is approximately the Mach number at which the pressure coefficient ahead of the wing began to increase (fig. 24). To generalize, it appears reasonable to expect the pressure coefficient due to a wing at a chord ahead of its tip to be small at low Mach numbers and to increase rapidly as the component of Mach number normal to the line of sweep exceeds appreciably the critical Mach number of the airfoil section.

At Mach numbers above the range of the measurements ($M>1.08$) it is reasonable to expect a variation of static-pressure error that is qualitatively similar to the theoretical variation; that is, the pressure coefficient should decrease slowly with Mach number. However, the pressure coefficient due to the wing should not be expected to decrease smoothly to zero at a Mach number of 1.25, as in the case of the theory, but to drop abruptly to zero at some Mach number

higher than 1.25 as the oblique bow wave from the wing-roo leading edge crosses behind the point of pressure measurement. It is important to remember that, after the passage of the wing bow wave, the point ahead of the wing will still lie in the positive pressure field of the fuselage nose and will continue to do so until after the passage of the fuselage bow wave at a Mach number in excess of 1.6.

CONCLUSIONS

The magnitude and variation of the static-pressure error for various distances ahead of sharp-nose bodies and open-nose air inlets for a distance of 1 chord ahead of the wing tip of a swept wing are defined by a combination of experiment and theory. The mechanism of the error is discussed in some detail to show the contributing factors that make up the error. The information presented provides a useful means for choosing a proper location for measurement of static pressure for most purposes.

The static-pressure error ahead of sharp-nose bodies, at Mach numbers below the critical Mach number of the body varies with position ahead of the body. The error is small at distances far ahead of the body and large at short distances ahead of the body. For Mach numbers above body critical Mach number, the error increases rapidly and, as in the case of Mach numbers below the body critical Mach number, the error varies inversely with position ahead of the body. At slightly supersonic Mach numbers, the bow wave from the body crosses the static-pressure orifices, and the error drops to zero and remains zero at higher Mach numbers.

The static-pressure error ahead of open-nose air inlets, at constant inlet-velocity ratio, is relatively independent of Mach number below a Mach number of 0.9 and varies inversely with distance ahead of the inlet. The variation throughout the Mach number range is similar to the variation ahead of sharp-nose bodies.

The static-pressure error at a distance of 1 tip chord ahead of the wing tip of a model of a swept-wing fighter airplane near zero lift was found to be essentially a function of the flow field of the fuselage and wing taken separately. The effect of the fuselage was negligible at Mach numbers below about 0.8. As the Mach number was increased above 0.8, however, the static-pressure error due to the fuselage became rapidly negative and reached a maximum near a Mach number of 1.0. Above a Mach number 1.0 the static-pressure error became less negative and approached zero at the highest Mach number of the investigation (Mach number 1.08). The static-pressure error due to the wing was negligible at Mach numbers below about 0.95. Between Mach numbers of 0.95 and 1.0, however, the static-pressure error became rapidly positive and remained constant to a Mach number of 1.08.

LANGLEY AERONAUTICAL LABORATORY,
NATIONAL ADVISORY COMMITTEE FOR AERONAUTICS,
LANGLEY FIELD, VA., *August 3, 1955.*

REFERENCES

1. Hensley, Reece V.: Calibrations of Pitot-Static Tubes at High Speeds. NACA WR L–396, 1942. (Formerly ACR, July 1942.)
2. Hasel, Lowell E., and Coletti, Donald E.: Investigation of Two Pitot-Static Tubes at Supersonic Speeds. NACA RM L8I02, 1948.
3. Gilruth, R. R., and Wetmore, J. W.: Preliminary Tests of Several Airfoil Models in the Transonic Speed Range. NACA ACR L5E08, 1945.
4. Letko, William: Investigation of the Fuselage Interference on a Pitot-Static Tube Extending Forward From the Nose of the Fuselage. NACA TN 1496, 1947.
5. Göthert, B.: Plane and Three-Dimensional Flow at High Subsonic Speeds. NACA TM 1105, 1946.
6. Danforth, Edward C. B., and Johnston, J. Ford: Pressure Distribution Over a Sharp-Nose Body of Revolution at Transonic Speeds by the NACA Wing-Flow Method. NACA RM L7K12, 1948.
7. Von Kármán, Theodore: The Similarity Law of Transonic Flow. Jour. Math. and Phys., vol. XXVI, no. 3, Oct. 1947, pp. 182–190.
8. Smith, Norman F.: Numerical Evaluation of Mass-Flow Coefficient and Associated Parameters from Wake-Survey Equations. NACA TN 1381, 1947.
9. Boswinkle, Robert W., Jr.: A Method for Calculating Flow Fields of Cowlings With Known Surface-Pressure Distributions. NACA RM L8I17, 1948.
10. Baals, Donald D., Smith, Norman F., and Wright, John B.: The Development and Application of High-Critical-Speed Nose Inlets. NACA Rep. 920, 1948. (Supersedes NACA ACR L5F30a.)
11. Jones, Robert T., and Margolis, Kenneth: Flow Over a Slender Body of Revolution at Supersonic Velocities. NACA TN 1081, 1946.
12. Jones, Robert T.: Subsonic Flow Over Thin Oblique Airfoils at Zero Lift. NACA Rep. 902, 1948. (Supersedes NACA TN 1340.)
13. Puckett, Allen E.: Supersonic Wave Drag of Thin Airfoils. Jour. Aero. Sci., vol. 13, no. 9, Sept. 1946, pp. 475–484.
14. Abbott, Ira H., Von Doenhoff, Albert E., and Stivers, Louis S., Jr.: Summary of Airfoil Data. NACA Rep. 824, 1945. (Supersedes NACA WR L–560.)